

Electrochemical synthesis and crystal structure of the organic ion intercalated superconductor $(\text{TMA})_{0.5}\text{Fe}_2\text{Se}_2$ with $T_c = 43$ K

Bettina Rendenbach, Timotheus Hohl, Sascha Harm, Constantin Hoch, and Dirk Johrendt*

Department Chemie, Ludwig-Maximilians-Universität München, Butenandtstr. 5–13 (Haus D),
81377 München, Germany

KEYWORDS. superconductivity; iron selenide; intercalation; electrolysis; crystal structure

ABSTRACT Intercalation of organic cations in superconducting iron selenide can significantly increase the critical temperature (T_c). We present an electrochemical method using β -FeSe crystals ($T_c \approx 8$ K) floating on mercury as cathode to intercalate tetramethyl ammonium ions (TMA^+) quantitatively and yielding bulk samples of $(\text{TMA})_{0.5}\text{Fe}_2\text{Se}_2$ with $T_c = 43$ K. The layered crystal structure is closely related to the ThCr_2Si_2 -type with disordered TMA^+ ions on the Th position between the FeSe layers. Although the organic ions are not detectable by X-ray diffraction, packing requirements as well as first principles DFT calculations constrain the specified structure. Our synthetic route enables electrochemical intercalations of other organic cations with high yields to greatly optimize the superconducting properties, and to expand this class of high- T_c materials.

In a superconductor electrons form pairs and electric currents flow dissipation-less below a critical temperature (T_c). Iron-based superconductors, discovered in 2008,^{1, 2} represent the second class of high-temperature superconductors beyond the copper oxides and attract tremendous interest equally in the physics and chemistry communities.³ While superconducting wires based on copper oxides currently begin to capture the market primarily in energy technologies,^{4, 5} iron-based superconductors are still in an early stage of innovation.^{6–8} Iron-based materials may outperform the copper oxides in a cost-effective production of round wires for high magnetic field applications,⁶ however, their critical temperature below the boiling point of liquid ammonia (77 K) is their main drawback. Indeed, after the discovery of superconductivity at 23 K in fluorine-doped $\text{LaO}_{1-x}\text{F}_x\text{FeAs}$,¹ T_c was raised quickly to 55 K in $\text{SmO}_{1-x}\text{F}_x\text{FeAs}$.⁹ But in spite of immense efforts for more than one decade, no bulk iron-based superconductor has reached the 77 K landmark so far. Only the finding of superconductivity up to 99 K¹⁰ in thin films of iron selenide β -FeSe proved the general potential for higher critical temperatures and fuels the

idea that this may also be possible in bulk materials, once the right composition and structure is found. The common structural trait of all iron-based superconductors are layers of edge-sharing $\text{FeX}_{4/4}$ tetrahedra (Fe^{2+} , $X = \text{As, Se}$), separated and charge balanced by interstitial atoms of various kinds. An impressive family of superconducting compounds¹¹ emerged by stacking of FeX layers with layers of alkaline,¹² alkaline-earth,¹³ or rare-earth ions,¹⁴ mixtures thereof,¹⁵ or with thicker perovskite-like oxide layers.¹⁶ Similar to the cuprates, superconductivity in FeX materials mostly emerges from a magnetic non-superconducting parent compound by chemical doping or applying high pressure. A special case is the β -polymorph of iron selenide FeSe , which is a superconductor below 8 K without doping.¹⁷ High pressure raises T_c of bulk β - FeSe to 36.7 K at 8.9 GPa,¹⁸ while one unit cell thin FeSe layers exhibit superconductivity up to 99 K.¹⁰ It has been shown that such high critical temperatures require doping of the FeSe layers by additional electrons transferred either from the $\text{Sr}(\text{Ti,Nb})\text{O}_3$ substrate¹⁹ or by potassium coating.²⁰ The critical temperature also increases in bulk β - FeSe by transfer of electrons through intercalation of cationic species in the van-der-Waals gap between the layers. Solid state reactions of β - FeSe with potassium yielded superconducting samples with T_c around 30 K,²¹ which turned out to be phase separated in strongly magnetic semiconducting $\text{K}_2\text{Fe}_4\text{Se}_5$, and superconducting K_xFeSe as main components.²² However, intercalation reactions with β - FeSe as host compound can proceed at low temperatures via soft chemistry methods.²³⁻²⁷ Examples are the intercalation of lithium ions together with amine and amide species in liquid ammonia ($(\text{Li}_x(\text{NH}_2)_y(\text{NH}_3)_{1-y})\text{Fe}_2\text{Se}_2$, $T_c = 43$ K),²⁸ of lithium hydroxide layers ($[(\text{Li}_{1-x}\text{Fe}_x)\text{OH}]\text{FeSe}$, $T_c = 42$ K)²⁹ by hydrothermal methods, or of alkaline ions with amine molecules ($(\text{Na}_{0.39}(\text{C}_2\text{N}_2\text{H}_8)_{0.77}\text{Fe}_2\text{Se}_2$, $T_c = 46$ K) by solvothermal reactions.²⁶ Another promising approach is the electrochemical intercalation of alkali metal ions. After the first report in 2010,³⁰ several studies state the formation of superconducting electrochemically intercalated FeSe compounds with critical temperatures around 40 ± 5 K.³¹⁻³³ A close inspection reveals that almost all of these materials suffer either from inhomogeneity, small superconducting volume fractions, or incomplete conversion of the host β - FeSe . Only recently, Shi et al. reported the electrochemical intercalation of large cetyl-trimethyl ammonium ions (CTA^+)^{34, 35} and tetrabutyl ammonium ions (TBA^+)³⁶ in individual β - FeSe crystals with superconducting transitions up to 50 K. A drawback of this method is the tiny sample amount, consisting of one crystal on the tip of an indium wire used as electrode. Furthermore, the current knowledge about the structures of the CTA^+ and TBA^+ intercalates is incomplete and limited to the distance between the FeSe layers so far,^{34, 36} while the detailed structure, even of the FeSe layers therein, remains unknown. Here, we demonstrate the electrochemical intercalation of tetramethyl-ammonium cations (TMA^+) into β -

FeSe. A modified setup of the electrochemical cell yields single phase bulk samples of $(\text{TMA})_{0.5}\text{Fe}_2\text{Se}_2$ with a superconducting transition at 43 K. We deduce a crystal structure closely related to the 122-type iron arsenide superconductors with ThCr_2Si_2 -type structure.

Single crystals of the host β -FeSe were prepared by chemical vapor transport as described in the literature.³⁷⁻³⁹ An optimized setup allows to grow about 1 gram β -FeSe crystals within one week. The quality of the host material was checked by powder X-ray diffraction of the crushed crystals and by magnetic susceptibility measurements. A portion of β -FeSe crystals were distributed on a drop of mercury in an amalgamated copper spoon as cathode.⁴⁰ The crystals float on the surface of the mercury ensuring the electrical contact, while they simultaneously bath in the electrolyte composed of tetramethyl ammonium iodide (TMAI) dissolved in dry DMF. For details, we refer to the supporting information. During the electrolysis the I^- in the electrolyte is oxidized to I_2 , while β -FeSe is reduced through intercalating TMA^+ ions. After the reaction is complete, the black polycrystalline and air-sensitive product is easy to separate from the mercury drop. Figure 1 shows the powder X-ray pattern with the Rietveld-fit. No impurity phases or residual β -FeSe are discernible within the limits of the method (≈ 1 wt. %). Some intensities slightly deviate, which is caused by the preferred orientation of the plate-like crystallites.

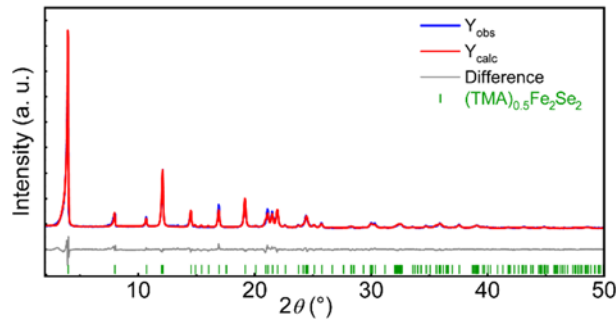


Figure 1. X-ray diffraction pattern of $(\text{TMA})_{0.5}\text{Fe}_2\text{Se}_2$ (blue) with Rietveld fit (red) and difference curve (grey).

The crystal structure was solved from the powder X-ray diffraction data in the space group $I4/mmm$ with lattice parameters $a = 3.8585(2)$ Å, $c = 20.377(3)$ Å. Only the iron and selenium atoms contribute significantly to the diffraction pattern, because CHN atoms are weak scatterer and the orientations of TMA^+ ions are disordered. However, the nitrogen atom in the center of the TMA^+ ion is not affected by the disorder and was included in the refinement, though its contribution is expectedly weak. Relevant crystallographic data are compiled in Table 1.

Table 1. Crystallographic data of (TMA)_{0.5}Fe₂Se₂ from Rietveld analysis

Space group	<i>I4/mmm</i> (139)					
Lattice parameters (Å)	<i>a</i> = 3.8585(2)					
	<i>c</i> = 20.377(3)					
Volume (Å³)	<i>V</i> = 303.4(1)					
<i>Z</i>	2					
Density (gcm ⁻³)	3.028(1)					
<i>R</i> _{exp} / <i>R</i> _{Bragg}	0.815/1.269					
<i>R</i> _p / <i>R</i> _{wp}	1.940/2.789					
GooF	3.423					
Atomic coordinates and isotropic displacement parameters						
Atom	Wyckoff	<i>x</i>	<i>y</i>	<i>z</i>	<i>SOF</i>	<i>B</i> _{iso}
Fe	4 <i>d</i>	0	½	¼	1	2.0(1)
Se	4 <i>e</i>	0	0	0.3160(4)	1	1.2(1)
N	2 <i>a</i>	0	0	0	0.5	3.9(1)
Bond distance (Å) and angle (°)						
Fe – 4 Se 2.352(3)			∠ Se-Fe-Se: 110.2(3)			

This atom configuration in the space group *I4/mmm* corresponds to the ThCr₂Si₂-type structure, known as the “122-type” structure of the iron arsenide superconductors.¹³ Even though the cavities in the structure around the N-atom sites at (0,0,0) and (½,½,½) appear large (Figure 2a), they are not large enough to be fully occupied by TMA⁺ ions. The encasing sphere of a tetrahedrally shaped TMA⁺ ion has a diameter of 5.5–5.6 Å^{41, 42} incompatible with the lattice parameter *a*, which is only 3.8585(2) Å. Indeed the diagonal of the unit cell $\sqrt{2}a = 5.457$ Å has the suitable size to accommodate neighboring TMA⁺ ions (Figure 2b), thus we assume that the positions (0,0,0) and (½,½,½) are statistically half occupied, resulting in the formula (TMA)_{0.5}Fe₂Se₂. This ordered model of the structure is shown in Figure 2c as ball-and-stick representation, and in Figure 2d with the van-der-Waals radii of the atoms. Figure 2e shows how the TMA⁺ ions almost perfectly fit in the $\sqrt{2}a \times \sqrt{2}a$ supercell. The space filling of this structure based on the van-der-Waals radii of the atoms calculated by PLATON⁴³ is as high as 77 %, similar to a typical compound with ThCr₂Si₂-type structure like BaFe₂As₂ which has a space filling of 82 %. Each two of the three hydrogen atoms at the -CH₃ groups form C-H...Se hydrogen bridges with a H...Se distance of 2.6(1) Å (Figure 2c), similar to the N-D...Se distance of 2.76 Å measured by Burrard-Lucas et al. in Li_x(ND₂)_y(ND₃)_{1-y}Fe₂Se₂ using neutron diffraction.²⁸ We do not expect more detailed

structural information from neutron data because of the orientation disorder of the TMA⁺ molecules, and since comparably disordered amine molecules between FeSe layers in Na_{0.39}(C₂N₂H₈)_{0.77}Fe₂Se₂ could not be localized by neutron diffraction.²⁶

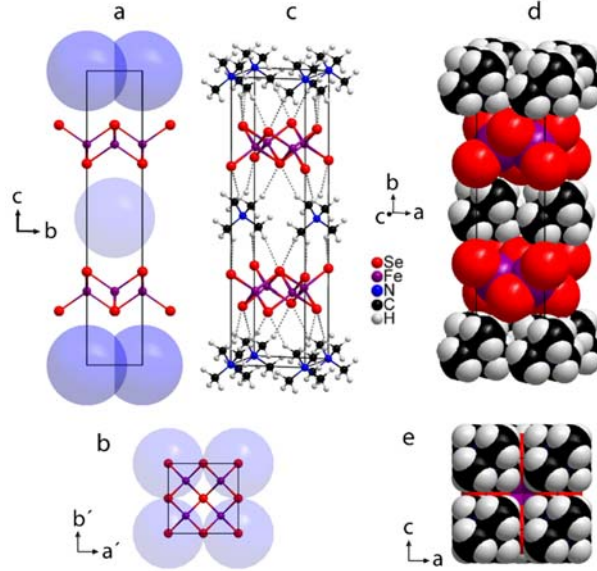


Figure 2. Crystal structure of (TMA)_{0.5}Fe₂Se₂. a: Structure determined from powder X-ray diffraction in space group *I4/mmm*. The interlayer distance is 10.2 Å; large blue spheres indicate the space around the nitrogen atoms required by a complete TMA⁺ ion. b: Doubled unit cell with $a' = \sqrt{2}a$, $b' = \sqrt{2}b$ with perfectly fitting TMA spheres. c: Complete structure of (TMA)_{0.5}Fe₂Se₂ in space group *C222* as ball-and-stick model with hydrogen bridges shown as dashed bonds. d: Space filling model based on van-der-Waals radii. e: View perpendicular to the TMA⁺ layers showing the dense packing of the cations.

We have checked the validity of our model by first-principle DFT calculations. Since DFT reproduces experimental structure data with deviations depending on the used functional, we have referenced the results to β -FeSe. For computational details see the supplemental information. The resulting structure data are given in Table S1, and a comparison with the experimental parameters of β -FeSe and (TMA)_{0.5}Fe₂Se₂ is in Table S2. The calculated bond lengths $d_{\text{Fe-Se}}$ and the lattice parameter a of (TMA)_{0.5}Fe₂Se₂ match the experimental values within $\pm 1.5\%$, while the c axis is within 3 % of the measured one. The latter is due to the weakness of DFT in treating dispersion interactions, which determine the interlayer distance. Nevertheless, all deviations from the experimental values are $< 4\%$, which clearly supports the structure. The assumed ordering of the TMA⁺ ions in the model, not present in the real structure, reduces the space group symmetry from *I4/mmm* to *C222*.

Chemical C-H-N analysis, EDS, and FT-IR spectroscopy confirm the composition $(\text{TMA})_{0.5}\text{Fe}_2\text{Se}_2$ within the errors of these methods, respectively. For details, we refer to the supplementary information. The intercalation is topotactic and reversible. High-temperature powder X-ray diffraction reveals the complete recovery of tetragonal β -FeSe after heating to 200 °C, and the transformation to the hexagonal polymorph at 550 °C (Figure 3).

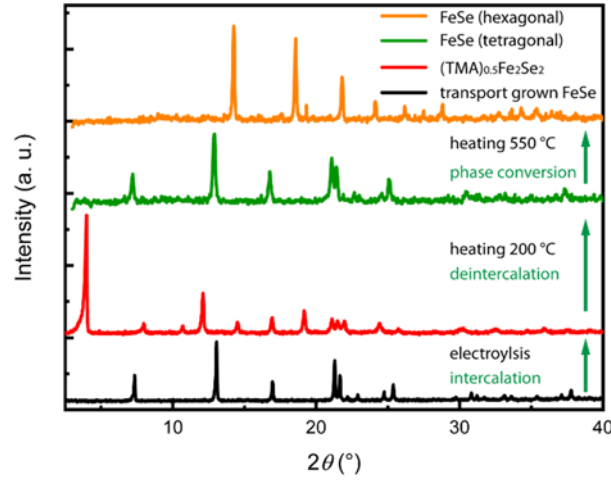


Figure 3. Powder X-ray diffraction patterns (Mo- $K_{\alpha 1}$ radiation) of the host β -FeSe (black), $(\text{TMA})_{0.5}\text{Fe}_2\text{Se}_2$ after electrochemical intercalation (red), recovered β -FeSe after deintercalation (green) and after phase conversion to hexagonal FeSe (orange).

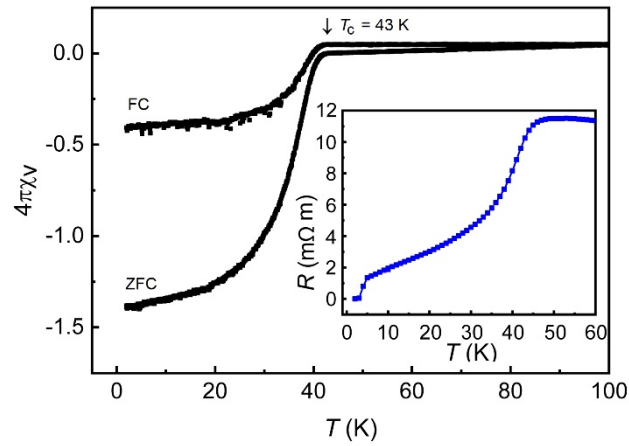


Figure 4. Magnetic susceptibility of $(\text{TMA})_{0.5}\text{Fe}_2\text{Se}_2$ at 15 Oe. Insert: DC resistivity of a cold pressed pellet.

The magnetic susceptibility of $(\text{TMA})_{0.5}\text{Fe}_2\text{Se}_2$ shows a bulk superconducting transition at 43 K (Figure 4). The large shielding fraction above 100 % at low temperatures comes from the uncorrected demagnetization of the plate-like crystallites oriented perpendicular to the magnetic field. Field-cooled and zero-field cooled curves slightly split above T_c due to traces of ferromagnetic impurities not detectable by X-ray diffraction. No further drop of the susceptibility near 8 K is visible, which confirms that the intercalation is complete and no residual host β -FeSe remains. Measuring the electrical resistivity turned out difficult due to degradation of the sample during pressing, and furthermore the deintercalation temperature around 200°C allowed no sintering of the pellet. The result is shown in the insert of Figure 4, where the onset of the superconductivity is near 45 K followed by a broad transition until an additional drop to zero resistivity occurs at 6 K. The latter is caused by ~ 8 wt.-% deintercalated FeSe. Isothermal magnetization measurements (Figure 5) show the “butterfly” pattern typical for a hard type-II superconductor. Whether the ripples in the curves are flux jumps or artefacts of the measurement is currently not clear and subject to further studies.

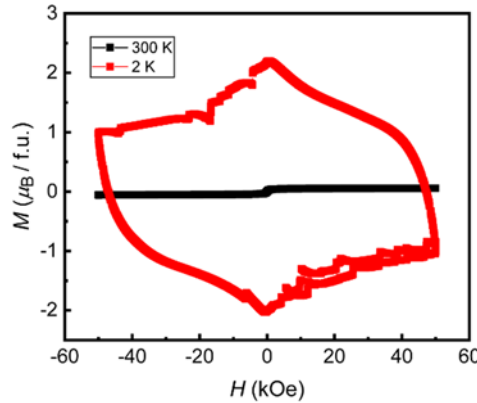


Figure 5. Magnetization isotherms of $(\text{TMA})_{0.5}\text{Fe}_2\text{Se}_2$ at 2 K and at 300 K.

In conclusion, we demonstrate that the electrochemical intercalation of tetramethyl ammonium ions (TMA^+) into the van-der-Waals gap of β -FeSe is feasible with high yields. Powder X-ray diffraction combined with DFT calculations reveal a plausible ordered model of the crystal structure. $(\text{TMA})_{0.5}\text{Fe}_2\text{Se}_2$ forms a variant of the ThCr_2Si_2 -type structure, also known as the “122-type” in the family of iron arsenide superconductors. The TMA^+ ions are closely packed between the FeSe layers, but disordered over two equivalent positions and in different orientations. Magnetization and electrical resistivity measurements show bulk superconducting transitions at 43 K, and identify $(\text{TMA})_{0.5}\text{Fe}_2\text{Se}_2$ as type-II superconductor. Our results provide first insights into the crystal structure of a superconducting FeSe-alkylammonium intercalate, and pave the way to further exploit the electrochemical route towards related compounds with potentially higher critical temperatures.

ASSOCIATED CONTENT

Supporting Information

Details about the synthesis, X-Ray powder diffraction data and Rietveld refinements, DFT-Calculations, HTPXRD, CHN elemental analysis, FT-IR spectroscopy, EDS data of the compound as well as additional figures and magnetic and resistivity data.

AUTHOR INFORMATION

Corresponding Author

Dirk Johrendt, Department Chemie, Ludwig-Maximilians-Universität München, Butenandtstr. 5–13 (Haus D), 81377 München, Germany

Author Contributions

The manuscript was written through contributions of all authors. / All authors have given approval to the final version of the manuscript.

Funding Sources

We gratefully acknowledge the financial support by the Deutsche Forschungsgemeinschaft (DFG), grant No. JO257/7-2

ACKNOWLEDGMENT

The authors thank the German Research Foundation (DFG- Deutsche Forschungsgemeinschaft) for funding this work (grant JO257/7-2). We thank Valentin Weippert for the magnetic and resistivity measurements, and Alan Virmani for the FT-IR measurements. The authors gratefully acknowledge the computational and data resources provided by the Leibniz Supercomputing Centre (www.lrz.de).

SUPPORTING INFORMATION

Details about the synthesis, structure determination by X-ray powder diffraction, DFT calculations, chemical analysis, magnetic measurements, and IR spectroscopy.

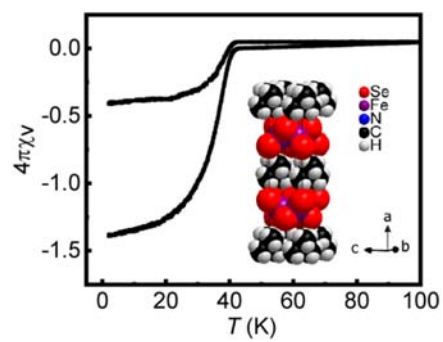
REFERENCES

1. Kamihara, Y.; Watanabe, T.; Hirano, M.; Hosono, H., Iron-Based Layered Superconductor $\text{La}[\text{O}_{1-x}\text{F}_x]\text{FeAs}$ ($x = 0.05\text{--}0.12$) with $T_c = 26$ K. *J. Am. Chem. Soc.* **2008**, 130, (11), 3296-3297.
2. Rotter, M.; Pangerl, M.; Tegel, M.; Johrendt, D., Superconductivity and Crystal Structures of $(\text{Ba}_{1-x}\text{K}_x)\text{Fe}_2\text{As}_2$ ($x = 0\text{--}1$). *Angew. Chem. Int. Ed.* **2008**, 47, (41), 7949-7952.
3. Si, Q.; Yu, R.; Abrahams, E., High-temperature superconductivity in iron pnictides and chalcogenides. *Nature Reviews Materials* **2016**, 1, 16017.
4. Bergen, A.; Andersen, R.; Bauer, M.; Boy, H.; Brake, M. t.; Brutsaert, P.; Bühner, C.; Dhallé, M.; Hansen, J.; ten Kate, H.; Kellers, J.; Krause, J.; Krooshoop, E.; Kruse, C.; Kylling, H.; Pilas, M.; Pütz, H.; Rebsdorf, A.; Reckhard, M.; Seitz, E.; Springer, H.; Song, X.; Tzabar, N.; Wessel, S.; Wiezoreck, J.; Winkler, T.; Yagotyntsev, K., Design and in-field testing of the world's first ReBCO rotor for a 3.6 MW wind generator. *Supercond. Sci. Technol.* **2019**, 32, (12), 125006.
5. Melhem, Z. E., *High Temperature Superconductors (HTS) for Energy Applications*. Woodhead Publishing Ltd.: 2012.
6. Yao, C.; Ma, Y., Recent breakthrough development in iron-based superconducting wires for practical applications. *Supercond. Sci. Technol.* **2019**, 32, (2), 023002.
7. Hosono, H.; Tanabe, K.; Takayama-Muromachi, E.; Kageyama, H.; Yamanaka, S.; Kumakura, H.; Nohara, M.; Hiramatsu, H.; Fujitsu, S., Exploration of new superconductors and functional materials, and fabrication of superconducting tapes and wires of iron pnictides. *Sci. Technol. Adv. Mater.* **2015**, 16, (3), 033503.
8. Hosono, H.; Yamamoto, A.; Hiramatsu, H.; Ma, Y., Recent advances in iron-based superconductors toward applications. *Materials Today* **2018**, 31, (3), 278-302.
9. Zestrea, V.; Kodash, V. Y.; Felea, V.; Petrenco, P.; Quach, D. V.; Groza, J. R.; Tsurkan, V., Structural and magnetic properties of FeCr_2S_4 spinel prepared by field-activated sintering and conventional solid-state synthesis. *J. Mater. Sci.* **2008**, 43, (2), 660-664.
10. Ge, J.-F.; Liu, Z.-L.; Liu, C.; Gao, C.-L.; Qian, D.; Xue, Q.-K.; Liu, Y.; Jia, J.-F., Superconductivity above 100 K in single-layer FeSe films on doped SrTiO_3 . *Nat Mater* **2015**, 14, (3), 285-289.
11. Stewart, G. R., Superconductivity in iron compounds. *Rev. Mod. Phys.* **2011**, 83, (4), 1589-1652.
12. Tapp, J. H.; Tang, Z. J.; Lv, B.; Sasmal, K.; Lorenz, B.; Chu, P. C. W.; Guloy, A. M., LiFeAs : An intrinsic FeAs-based superconductor with $T_c=18$ K. *Phys. Rev. B* **2008**, 78, (6), 060505.
13. Rotter, M.; Tegel, M.; Johrendt, D., Superconductivity at 38 K in the iron arsenide $(\text{Ba}_{1-x}\text{K}_x)\text{Fe}_2\text{As}_2$. *Phys. Rev. Lett.* **2008**, 101, (10), 107006.
14. Ren, Z. A.; Che, G. C.; Dong, X. L.; Yang, J.; Lu, W.; Yi, W.; Shen, X. L.; Li, Z. C.; Sun, L. L.; Zhou, F.; Zhao, Z. X., Superconductivity and phase diagram in iron-based arsenic-oxides $\text{ReFeAsO}_{(1-\delta)}$ (Re = rare-earth metal) without fluorine doping. *Epl* **2008**, 83, (1), 4.
15. Iyo, A.; Kawashima, K.; Kinjo, T.; Nishio, T.; Ishida, S.; Fujihisa, H.; Gotoh, Y.; Kihou, K.; Eisaki, H.; Yoshida, Y., New-Structure-Type Fe-Based Superconductors: $\text{CaAFe}_4\text{As}_4$ ($A = \text{K, Rb, Cs}$) and $\text{SrAFe}_4\text{As}_4$ ($A = \text{Rb, Cs}$). *J. Am. Chem. Soc.* **2016**, 138, (10), 3410-3415.

16. Zhu, X.; Han, F.; Mu, G.; Cheng, P.; Shen, B.; Zeng, B.; Wen, H.-H., Transition of stoichiometric $\text{Sr}_2\text{VO}_3\text{FeAs}$ to a superconducting state at 37.2 K. *Phys. Rev. B* **2009**, 79, (22), 220512-4.
17. Hsu, F.-C.; Luo, J.-Y.; Yeh, K.-W.; Chen, T.-K.; Huang, T.-W.; Wu, P. M.; Lee, Y.-C.; Huang, Y.-L.; Chu, Y.-Y.; Yan, D.-C.; Wu, M.-K., Superconductivity in the PbO-type structure α -FeSe. *Proc. Natl. Acad. Sci. U.S.A.* **2008**, 105, (38), 14262–14264.
18. Medvedev, S.; McQueen, T. M.; Troyan, I. A.; Palasyuk, T.; Eremets, M. I.; Cava, R. J.; Naghavi, S.; Casper, F.; Ksenofontov, V.; Wortmann, G.; Felser, C., Electronic and magnetic phase diagram of beta-Fe_{1.01}Se with superconductivity at 36.7 K under pressure. *Nat. Mater.* **2009**, 8, (8), 630-633.
19. Zhou, Y. J.; Millis, A. J., Charge transfer and electron-phonon coupling in monolayer FeSe on Nb-doped SrTiO₃. *Phys. Rev. B* **2016**, 93, (22), 8.
20. Miyata, Y.; Nakayama, K.; Sugawara, K.; Sato, T.; Takahashi, T., High-temperature superconductivity in potassium-coated multilayer FeSe thin films. *Nat Mater* **2015**, 14, (8), 775-779.
21. Guo, J. G.; Jin, S. F.; Wang, G.; Wang, S. C.; Zhu, K. X.; Zhou, T. T.; He, M.; Chen, X. L., Superconductivity I n the iron selenide $\text{K}_x\text{Fe}_2\text{Se}_2$ ($0 \leq x \leq 1.0$). *Phys. Rev. B* **2010**, 82, (18), 180520.
22. Shoemaker, D. P.; Chung, D. Y.; Claus, H.; Francisco, M. C.; Avci, S.; Llobet, A.; Kanatzidis, M. G., Phase relations in $\text{K}_x\text{Fe}_{2-y}\text{Se}_2$ and the structure of superconducting $\text{K}_x\text{Fe}_2\text{Se}_2$ via high-resolution synchrotron diffraction. *Phys. Rev. B* **2012**, 86, (18), 184511.
23. Krzton-Maziopa, A.; Pesko, E.; Puzniak, R., Superconducting selenides intercalated with organic molecules: synthesis, crystal structure, electric and magnetic properties, superconducting properties, and phase separation in iron based-chalcogenides and hybrid organic-inorganic superconductors. *J. Phys. Condens. Matter* **2018**, 30, (24), 243001.
24. Dong, X.; Zhou, H.; Yang, H.; Yuan, J.; Jin, K.; Zhou, F.; Yuan, D.; Wei, L.; Li, J.; Wang, X.; Zhang, G.; Zhao, Z., Phase Diagram of $(\text{Li}_{1-x}\text{Fe}_x)\text{OHFeSe}$: A Bridge between Iron Selenide and Arsenide Superconductors. *J. Am. Chem. Soc.* **2015**, 137, (1), 66-69.
25. Sun, R.; Jin, S.; Gu, L.; Zhang, Q.; Huang, Q.; Ying, T.; Peng, Y.; Deng, J.; Yin, Z.; Chen, X., Intercalating Anions between Terminated Anion Layers: Unusual Ionic S–Se Bonds and Hole-Doping Induced Superconductivity in $\text{S}_{0.24}(\text{NH}_3)_{0.26}\text{Fe}_2\text{Se}_2$. *J. Am. Chem. Soc.* **2019**, 141, (35), 13849–13857.
26. Jin, S.; Fan, X.; Wu, X.; Sun, R.; Wu, H.; Huang, Q.; Shi, C.; Xi, X.; Li, Z.; Chen, X., High-T_c superconducting phases in organic molecular intercalated iron selenides: synthesis and crystal structures. *Chem. Commun.* **2017**, 53, (70), 9729-9732.
27. Xu, H.-S.; Wang, X.-X.; Tang, L.-L.; Yang, K.-P.; Yang, D.; Long, Y.-Z.; Tang, K.-B., New Synthetic Route to Synthesize Li and 1,2-Diaminopropane-Intercalated Iron-Based Superconductor with T_c=37 K. *ChemistrySelect* **2018**, 3, (27), 7757–7762.
28. Burrard-Lucas, M.; Free, D. G.; Sedlmaier, S. J.; Wright, J. D.; Cassidy, S. J.; Hara, Y.; Corkett, A. J.; Lancaster, T.; Baker, P. J.; Blundell, S. J.; Clarke, S. J., Enhancement of the superconducting transition temperature of FeSe by intercalation of a molecular spacer layer. *Nat. Mater.* **2013**, 12, 15-19.
29. Pachmayr, U.; Nitsche, F.; Luetkens, H.; Kamusella, S.; Brückner, F.; Sarkar, R.; Klauss, H.-H.; Johrendt, D., Coexistence of 3d-Ferromagnetism and Superconductivity in $[(\text{Li}_{1-x}\text{Fe}_x)\text{OH}](\text{Fe}_{1-y}\text{Li}_y)\text{Se}$. *Angew. Chem. Int. Ed.* **2015**, 54, (1), 293-297.

30. Abe, H.; Noji, T.; Kato, M.; Koike, Y., Electrochemical Li-intercalation into the Fe-based superconductor $\text{FeSe}_{1-x}\text{Te}_x$. *Physica C* **2010**, 470, S487–S488.
31. Kajita, T.; Kawamata, T.; Noji, T.; Hatakeda, T.; Kato, M.; Koike, Y.; Itoh, T., Electrochemical Na-intercalation-induced high-temperature superconductivity in FeSe. *Physica C* **2015**, 519, 104–107.
32. Shen, S.-J.; Ying, T.-P.; Wang, G.; Jin, S.-F.; Zhang, H.; Lin, Z.-P.; Chen, X.-L., Electrochemical synthesis of alkali-intercalated iron selenide superconductors. *Chinese Physics B* **2015**, 24, (11), 117406.
33. Alekseeva, A. M.; Drozhzhin, O. A.; Dosaev, K. A.; Antipov, E. V.; Zakharov, K. V.; Volkova, O. S.; Chareev, D. A.; Vasiliev, A. N.; Koz, C.; Schwarz, U.; Rosner, H.; Grin, Y., New superconductor $\text{Li}_x\text{Fe}_{1+\delta}\text{Se}$ ($x \leq 0.07$, T_c up to 44 K) by an electrochemical route. *Scientific Reports* **2016**, 6, (1), 25624.
34. Shi, M. Z.; Wang, N. Z.; Lei, B.; Shang, C.; Meng, F. B.; Ma, L. K.; Zhang, F. X.; Kuang, D. Z.; Chen, X. H., Organic-ion-intercalated FeSe-based superconductors. *Physical Review Materials* **2018**, 2, (7), 074801.
35. Sun, J. P.; Shi, M. Z.; Lei, B.; Xu, S. X.; Uwatoko, Y.; Chen, X. H.; Cheng, J. G., Pressure-induced second high- T_c superconducting phase in the organic-ion-intercalated $(\text{CTA})_{0.3}\text{FeSe}$ single crystal. *EPL-Europhys. Lett.* **2020**, 130, (6), 67004.
36. Shi, M. Z.; Wang, N. Z.; Lei, B.; Ying, J. J.; Zhu, C. S.; Sun, Z. L.; Cui, J. H.; Meng, F. B.; Shang, C.; Ma, L. K.; Chen, X. H., FeSe-based superconductors with a superconducting transition temperature of 50 K. *New J. Phys.* **2018**, 20, (12), 123007.
37. Böhmer, A. E.; Hardy, F.; Eilers, F.; Ernst, D.; Adelman, P.; Schweiss, P.; Wolf, T.; Meingast, C., Lack of coupling between superconductivity and orthorhombic distortion in stoichiometric single-crystalline FeSe. *Phys. Rev. B* **2013**, 87, (18), 180505.
38. Böhmer, A. E.; Taufour, V.; Straszheim, W. E.; Wolf, T.; Canfield, P. C., Variation of transition temperatures and residual resistivity ratio in vapor-grown FeSe. *Phys. Rev. B* **2016**, 94, (2), 024526.
39. Chareev, D.; Osadchii, E.; Kuzmicheva, T.; Lin, J.-Y.; Kuzmichev, S.; Volkova, O.; Vasiliev, A., Single crystal growth and characterization of tetragonal FeSe_{1-x} superconductors. *CrystEngComm* **2013**, 15, (10), 1989–1993.
40. Tambornino, F.; Sappl, J.; Pultar, F.; Cong, T. M.; Hübner, S.; Giftthaler, T.; Hoch, C., Electrocrystallization: A Synthetic Method for Intermetallic Phases with Polar Metal–Metal Bonding. *Inorg. Chem.* **2016**, 55, (21), 11551–11559.
41. Gao, Q.; Giraldo, O.; Tong, W.; Suib, S. L., Preparation of Nanometer-Sized Manganese Oxides by Intercalation of Organic Ammonium Ions in Synthetic Birnessite OL-1. *Chem. Mater.* **2001**, 13, (3), 778–786.
42. Liu, Z.-h.; Wang, Z.-M.; Yang, X.; Ooi, K., Intercalation of Organic Ammonium Ions into Layered Graphite Oxide. *Langmuir* **2002**, 18, (12), 4926–4932.
43. Spek, A., Single-crystal structure validation with the program PLATON. *J. Appl. Crystallogr.* **2003**, 36, (1), 7–13.

Table of Contents



Supporting Information

1. Synthesis

(TMA)_{0.5}Fe₂Se₂ (TMA = tetramethylammonium, NC₄H₁₂⁺) was synthesized by electrochemical intercalation of tetramethylammonium iodide into iron selenide crystals. The host compound β -FeSe was synthesized with chemical vapour-transport.¹ 562.4 mg Se powder (Chempur, 99.9 %) and 437.8 mg Fe powder (CHEMPUR, 99.9 %) in a molar ratio 1 : 1.1 were ground together with AlCl₃/KCl (ALFA AESAR, 99.985 % / GRÜSSING, 99.5 %, dried) (7.75 g : 2.25 g). The mixture was sealed under vacuum in a glass ampoule (diameter 5 cm, length 4 cm) and placed in a vertical two-zone furnace and heated to 390 °C at the bottom and 290 °C at the top. This temperature gradient was held for 5–10 days.² After cooling the ampoules were opened and the crystals collected from the inner top of the ampoules.

The electrochemical cell consisted of a tungsten anode and an amalgamated copper spoon connected to a platinum wire as cathode. A drop of mercury was added to the spoon.² On top of this drop the polycrystalline powder of β -FeSe was distributed. The apparatus was held under inert conditions using purified argon. The electrolyte consisted of tetramethylammonium iodide (TMAI, SIGMA-ALDRICH, 99 %, 0.1 molar) dissolved in 100 mL dried and distilled DMF. A voltage of 3 V was applied for 3–4 days. After the reaction the product was washed with dry DMF and dried under vacuum.

2. Powder X-ray diffraction

Glass capillaries (0.3 mm in diameter, Hilgenberg GmbH) were filled with the samples and sealed. A Stoe Stadi-P diffractometer (MoK α 1, Ge(111)-monochromator, Mythen 1k detector) was used to measure the patterns which were analysed and fitted using the Topas package.^{3,4} After indexing the data with the SVG-algorithm, the space group *I4/mmm* was chosen.⁵ Intensities were gathered using the Pawley method, and the structure was solved by charge-flipping.^{3,6,7} The trial structures were used in subsequent Rietveld refinements and visualized by the program Diamond.⁸

Measurements at high temperatures performed on samples in silica capillaries (diameter 0.5 mm, Hilgenberg GmbH, sealed with grease) on a Stoe Stadi-P diffractometer (MoK α , Ge(111)-monochromator, IP-PSD detector) equipped with a graphite furnace. Data were visualized with WinXPOW.⁹

3. DFT calculations

First-principles electronic structure calculations were performed using the Vienna ab initio simulation package (VASP 5.4.4)^{10,11} based on density functional theory (DFT) and plane wave basis sets. Projector-augmented waves

(PAW)¹² were used and contributions of correlation and exchange were treated using the strongly constrained and appropriately normed semilocal density functional (SCAN).¹³ Corrections for dispersion were applied using the zero damping DFT-D3 method of Grimme.¹⁴ The k -space was sampled with the Monkhorst-Pack¹⁵ scheme using an $11 \times 11 \times 11$ grid based on the primitive unit cell. The AFLOW¹⁶ utilities were used to transform between primitive and conventional unit cells, and FINDSYM¹⁷ to determine the space group symmetry. Convergence criteria were 10^{-7} eV for the total energy and 10^{-5} eV for the structural relaxations regarding ion positions and unit cell changes using a plane wave cut-off energy of 600 eV. The parameters of the fully relaxed structure of (TMA)_{0.5}Fe₂Se₂ in the space group C222 are compiled in Table S1.

Table S1. DFT-optimized structure data of (TMA)_{0.5}Fe₂Se₂ with experimental values in square brackets.

Crystal system	Orthorhombic			
Space group	C222 (No. 21)			
	$a = 5.386$ [5.457]			
	$b = 20.934$ [20.377]			
Lattice parameters (Å)	$c = 5.386$ [5.457]			
Volume (Å³)	606.74 [606.7]			
Z	4			
Atom positions				
Atom	Wyckoff	x	Y	z
Se1	$4e$	0	0.6818 [0.6840]	0
Se2	$4f$	0	0.1820 [0.1840]	$\frac{1}{2}$
Fe1	$4k$	$\frac{1}{4}$	$\frac{1}{4}$	0.2500 [$\frac{1}{4}$]
Fe2	$4k$	$\frac{1}{4}$	$\frac{1}{4}$	0.7500 [$\frac{3}{4}$]
N	$2a$	0 [0]	0 [0]	0 [0]
C	$8l$	0.6593	0.4587	0.1591
H1	$8l$	0.2839	0.0102	0.7263
H2	$8l$	0.0419	0.0718	0.7266
H3	$8l$	0.2739	0.0719	0.9579

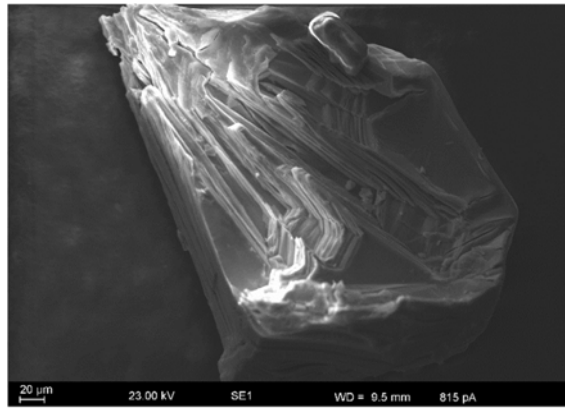
Table S2. Experimental and calculated structure parameters for FeSe and (TMA)_{0.5}Fe₂Se₂

	a (Å)	$\frac{\Delta a}{a}$ %	c (Å)	$\frac{\Delta c}{c}$ %	V (Å ³)	$\frac{\Delta V}{V}$ %	d_{FeSe} (Å)	$\frac{\Delta d}{d}$ %	φ (°)	$\frac{\Delta \varphi}{\varphi}$ %
β -FeSe (exp)	3.772		5.524		78.59		2.393		104.0	
β -FeSe (calc)	3.778	+0.16	5.506	-0.33	77.60	+0.01	2.378	-0.63	105.2	+1.15
(TMA) _{0.5} Fe ₂ Se ₂ (exp)	5.457*		20.377		606.75		2.352		110.2	
(TMA) _{0.5} Fe ₂ Se ₂ (calc)	5.384	-1.33	20.934	+2.7	606.7	+0.01	2.379	+1.14	106.3	-3.54

*Experimental lattice parameter a $(3.8383) \times \sqrt{2}$

4. Chemical analysis

CHN elemental analysis and energy-dispersive spectroscopy measurements (EDS) confirm the chemical composition (TMA)_{0.5}Fe₂Se₂ (see Tables S3 and S4). Figure S1 shows the morphology of a crystallite after intercalation. EDS measurements were performed on a Carl Zeiss Evo-Ma10 microscope with a Bruker Nano EDX detector (X-Flash detector 410 M). The controlling software is SmartSem for the detectors (SE and BSE)¹⁸ and for the collections and evaluation of the spectra the program QUANTAX 200 was used.¹⁹ Any elements from the sample holder and the adhesive carbon pads were discounted.

**Figure S1.** SEM image of (TMA)_{0.5}Fe₂Se₂.**Table S3.** C:N:H ratios from elemental analysis normalized to N = 1.

	C	H	N
(TMA) _{0.5} Fe ₂ Se ₂	4.1	13.1	1

Table S4. Fe : Se ratio from EDS normalized to Se.

	Fe	Se
(TMA) _{0.5} Fe ₂ Se ₂	1.1(1)	1.0(1)

The molar ratio of C : H : N was determined to be 4.1 : 13.1 : 1 which is consistent with C₄NH₁₂⁺ and confirms the integrity of the TMA⁺ ion. The CHN elemental analysis was single determined and therefore no standard deviations are given. The CHN mass fraction with respect to FeSe was 12.02 %. This corresponds to a value of 0.24 TMA⁺ molecules per FeSe and confirms the composition (TMA)_{0.5}Fe₂Se₂.

5. Magnetic and resistivity Measurements

Magnetic measurements of β -FeSe and (TMA)_{0.5}Fe₂Se₂ were carried out on a Physical Property Measurement System (PPMS-9, Quantum Design) with a vibrating sample magnetometer (VSM). Zero-field cooled and field-cooled measurements were conducted between 2 K and 100 K and an applied field of 15 Oe. The isothermal magnetization was measured at 2 K and 300 K ($H = \pm 50$ kOe). For the resistivity measurements, the samples were ground and pressed into pellets (diameter 5 mm, thickness ~ 0.8 mm). The pellets were contacted with the Wimbush press contact assembly for van der Pauw measurements.^{19, 20}

6. Infrared Spectroscopy

FT-IR spectra were measured on a Bruker Vertex-80V FT-IR spectrometer ($\tilde{\nu} = 350 - 4000$ cm⁻¹). Figure S2 shows the spectra of tetramethylammonium iodide (TMAI) and (TMA)_{0.5}Fe₂Se₂. FeSe is not infrared active. The TMA⁺ ion has T_d symmetry, and 7 of the 19 fundamental vibrations are infrared active.²¹ Raman measurements were not possible due to the strong absorption of the product (black color).

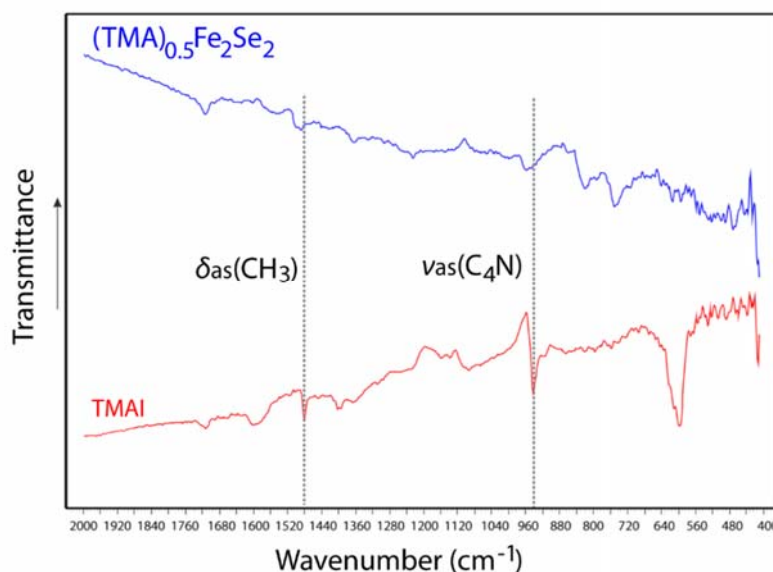


Figure S2. FT-IR spectra of TMAI and $(\text{TMA})_{0.5}\text{Fe}_2\text{Se}_2$.

In our structure model of $(\text{TMA})_{0.5}\text{Fe}_2\text{Se}_2$ the TMA^+ ions are located between FeSe layers. Therefore, in comparison to TMAI, the infrared active species in our samples are strongly diluted by the strong IR absorber FeSe. This may be the main factor for the weak intensity of the bands in the spectra. The FT-IR spectra of TMAI and $(\text{TMA})_{0.5}\text{Fe}_2\text{Se}_2$ are nevertheless compatible with intercalation of TMA^+ into FeSe. This indicates the asymmetric deformations mode vibrations of the methyl group $\delta_{\text{as}}(\text{CH}_3)$ at 1481 cm^{-1} and 1501 cm^{-1} in both spectra (TMAI and $(\text{TMA})_{0.5}\text{Fe}_2\text{Se}_2$), respectively. The bands are in accordance with literature and only a slight shift to higher wavenumber is apparent (1483 cm^{-1}).²² Furthermore, around 958 cm^{-1} a band is visible in both spectra, which could be assigned to the asymmetric stretching mode of the skeletal C_4N . The strong band at $\sim 600\text{ cm}^{-1}$ in the TMAI spectra might be assigned to methyl iodide which could originate from a side reaction during the measurement process. This band is not visible in the product spectrum.

7. Deintercalation of $(\text{TMA})_{0.5}\text{Fe}_2\text{Se}_2$

A $(\text{TMA})_{0.5}\text{Fe}_2\text{Se}_2$ sample was heated to $200\text{ }^\circ\text{C}$ for 4 h under argon atmosphere. The residual black powder was analyzed by powder diffraction and magnetic measurements. The powder pattern revealed single phase $\beta\text{-FeSe}$ (see Figure S3), thus $(\text{TMA})_{0.5}\text{Fe}_2\text{Se}_2$ has been quantitatively deintercalated.

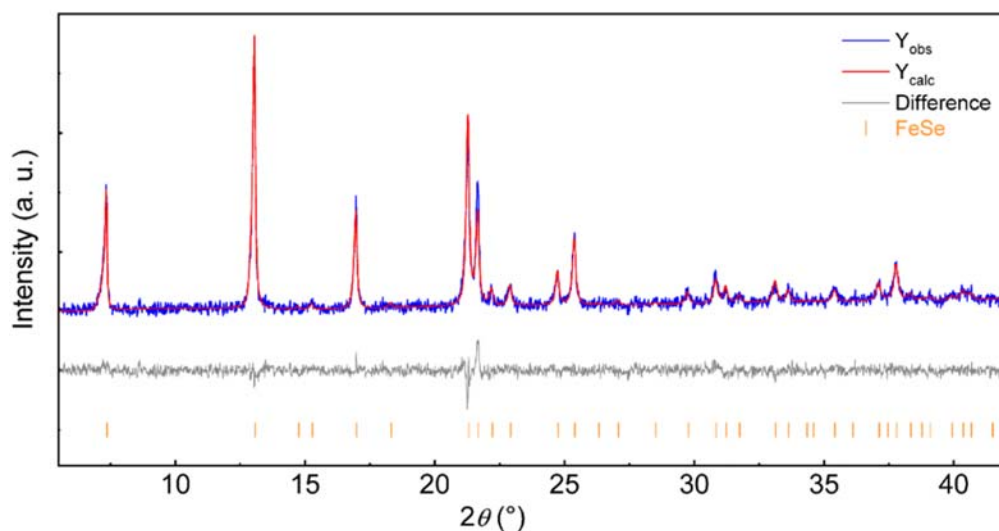


Figure S3. PXRD pattern of the residue after heating at 200 °C with Rietveld fit (red) and the difference curve (grey).

The regained β -FeSe has the same lattice parameters (3.771(3) and 5.524(7) Å) as the starting material. The susceptibilities curves show that the regained β -FeSe is superconducting at 8 K, which is consistent with the original properties of β -FeSe (see Figure S4).

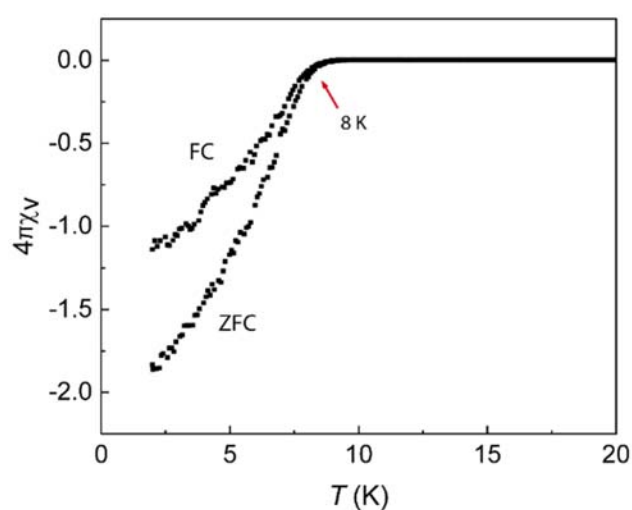


Figure S4. Magnetic susceptibility of the residue after heating. FC is field cooled and ZFC is zero-field cooled.

SI References

1. Chareev, D.; Osadchii, E.; Kuzmicheva, T.; Lin, J.-Y.; Kuzmichev, S.; Volkova, O.; Vasiliev, A., Single crystal growth and characterization of tetragonal FeSe_{1-x} superconductors. *CrystEngComm* **2013**, 15, (10), 1989–1993.
2. Tambornino, F.; Sappl, J.; Pultar, F.; Cong, T. M.; Hübner, S.; Giftthaler, T.; Hoch, C., Electrocrystallization: A Synthetic Method for Intermetallic Phases with Polar Metal–Metal Bonding. *Inorg. Chem.* **2016**, 55, (21), 11551–11559.

3. Coelho, A., *TOPAS-Academic*. Version 4.1, Coelho Software: Brisbane, Australia, 2007.
4. Coelho, A. *TOPAS Academics*, 6; Coelho Software: Brisbane, Australia, 2016.
5. Coelho, A., Indexing of powder diffraction patterns by iterative use of singular value decomposition. *J. Appl. Crystallogr.* **2003**, 36, (1), 86–95.
6. Pawley, G., Unit-cell refinement from powder diffraction scans. *J. Appl. Crystallogr.* **1981**, 14, (6), 357–361.
7. Oszlanyi, G.; Suto, A., The charge flipping algorithm. *Acta Crystallogr. Sec. A* **2008**, 64, (1), 123–134.
8. Brandenburg, K. *Diamond*, 3.2k; Crystal Impact GbR: Bonn, Germany, 2014.
9. *WinXPOW*, Version 3.0.2.5; STOE & Cie GmbH: Darmstadt, Germany, 2011.
10. Kresse, G.; Furthmüller, J., Efficient iterative schemes for ab initio total-energy calculations using a plane-wave basis set. *Phys. Rev. B* **1996**, 54, (16), 11169–11186.
11. Kresse, G.; Furthmüller, J., Efficiency of ab-initio total energy calculations for metals and semiconductors using a plane-wave basis set. *Comput. Mater. Sci.* **1996**, 6, (1), 15–50.
12. Kresse, G.; Joubert, D., From ultrasoft pseudopotentials to the projector augmented-wave method. *Phys. Rev. B* **1999**, 59, (3), 1758–1775.
13. Sun, J.; Ruzsinszky, A.; Perdew, J. P., Strongly Constrained and Appropriately Normed Semilocal Density Functional. *Phys. Rev. Lett.* **2015**, 115, (3), 036402.
14. Grimme, S.; Antony, J.; Ehrlich, S.; Krieg, H., A consistent and accurate ab initio parametrization of density functional dispersion correction (DFT-D) for the 94 elements H–Pu. *The Journal of Chemical Physics* **2010**, 132, (15), 154104.
15. Monkhorst, H. J.; Pack, J. D., Special points for Brillouin-zone integrations. *Phys. Rev. B* **1976**, 13, (12), 5188–5192.
16. Setyawan, W.; Curtarolo, S., High-throughput electronic band structure calculations: Challenges and tools. *Comput. Mat. Sci.* **2010**, 49, (2), 299–312.
17. Stokes, H. T.; Hatch, D. M., FINDSYM: program for identifying the space-group symmetry of a crystal. *J. Appl. Crystallogr.* **2005**, 38, (1), 237–238.
18. *SmartSEM*, Version 5.07 Beta; Carl Zeiss Microscopy Ltd.: Cambridge, UK, 2014.
19. *QUANTAX 200*, Version 1.9.4.3448; Bruker Nano GmbH: Berlin, Germany, 2013.
20. *MultiVu*, Version 1.5.11; Quantum Design Inc.: San Diego, USA, 2013.
21. Bottger, G. L.; Geddes, A. L., The infrared spectra of the crystalline tetramethylammonium halides. *Spectrochim. Acta* **1965**, 21, (10), 1701–1708.
22. Kornath, A.; Blecher, O.; Neumann, F.; Ludwig, R., Vibrational spectra of the tetramethylpnikogenonium ions. *J. Mol. Spectrosc.* **2003**, 219, (1), 170–174.